journal

J. Am. Ceram. Soc., 94 [9] 3123–3130 (2011)
DOI: 10.1111/j.1551-2916.2011.04486.x


# A Raman Study of Iron–Phosphate Crystalline Compounds and Glasses

Liying Zhang* and Richard K. Brow*,†

Department of Materials Science and Engineering, Missouri University of Science and Technology, Rolla 65409, Missouri

**Ferrous and ferric phosphate crystalline compounds and glasses were studied using Raman spectroscopy. A comparison of the spectra from crystalline and glassy ortho-, pyro-, and metaphosphates indicates that similar phosphate anions constitute the structures of the respective materials, and some information about the compositional dependence of the phosphate-site distributions in the glasses can be gleaned from relative peak intensities. A correlation exists between the average P–O bond distance and the Raman peak frequencies in the crystalline compounds, and this correlation is used to provide information about the structures of the iron phosphate glasses. For example, the average P–O bond distance is estimated to decrease from about 1.57 Å for iron metaphosphate glasses (O/P ~ 3.0) to 1.54 Å for iron orthophosphate glasses (O/P ~ 4.0). These bond distances are in good agreement with those reported from diffraction studies of similar glasses.**

## I. Introduction

Crystalline and amorphous iron phosphate materials are being developed for a variety of technological applications. For example, amorphous and crystalline $FePO_4$ and similar compounds have been developed as catalysts,[1] and the catalytic performance is affected by reduction to $Fe_2P_2O_7$.[2] $LiFePO_4$ has been proposed as a cathode material for rechargeable Li-ion batteries[3,4] and the dilithiation process can form disordered products that are sometimes difficult to characterize by conventional diffraction techniques. The ferric oxo-phosphate phase $Fe_3PO_7$ has also been evaluated as a potential electrode material.[5]

Iron phosphate glasses are of interest for a variety of applications, including as corrosion resistant hosts for radioactive wastes.[6–9] Typical iron phosphate glasses for waste applications are based on a ferric pyrophosphate ($40Fe_2O_3$–$60P_2O_5$ molar) nominal composition in which some fraction of ferric ions reduce to ferrous ions, to yield a structure based on ferric and ferrous polyhedra that link various phosphate anions.[8,9] The properties of these glasses are sensitive to changes in iron valence and the Fe/P ratio, both of which affect the overall O/P ratio, which determines the distribution of phosphate anions. Glasses with O/P ~ 3 are classified as metaphosphates and possess relatively long chains of P-tetrahedra that link neighboring tetrahedra through two bridging oxygens; these tetrahedra are sometimes classified as $Q^2$-tetrahedra.[10] The chains are terminated by phosphate units with a single bridging oxygen ($Q^1$ units). A pyrophosphate composition (O/P ~ 3.5) could have a structure based principally on $Q^1$-tetrahedra that form $P_2O_7^{4-}$ anions. Compositions with O/P > 3.5 will have structures based on $Q^1$- and $Q^0$-tetrahedra; the latter are similar to isolated (no bridging oxygens) phosphate tetrahedra found in crystalline orthophosphate compounds.

Raman spectroscopy has been widely used to provide information about the anions that constitute the structures of phosphate glasses and crystals.[11–34] The frequency of the P–O-stretching vibrations changes systematically with the number of bridging oxygens ($Q^x$) on a tetrahedron, and so Raman peaks associated with the different P–O vibrational modes can be used to identify different structural elements. Rulmont *et al.*[15] compared the Raman and IR spectra of pyro- and metaphosphate materials and showed that crystalline and glassy phosphates with similar compositions have similar phosphate anions. In addition, more quantitative information about the structures of crystalline and glassy phosphates, including estimates of P–O bond lengths and P–O–P bond angles, can be obtained from Raman peak positions.[15,16]

There have been several Raman studies of iron phosphate glasses.[17–19] The compositions studied were generally limited to those near the pyrophosphate stoichiometry of interest for waste vitrification applications. Qualitative changes in peak shapes and positions have been related to glass compositions, but little detailed information has been reported. In the present study, the Raman spectra of 10 crystalline ferric, ferrous, and mixed ferric-ferrous phosphate compounds, including ortho- (O/P = 4.0, $Q^0$), pyro- (O/P = 3.5, $Q^1$), and metaphosphate (O/P = 3.0, $Q^2$) compounds, were collected, and those results are used to interpret the Raman spectra of iron phosphate glasses with a wide variety of O/P and Fe/P ratios to provide information about phosphate tetrahedral distributions and estimates of P–O bond lengths for a much broader range of iron phosphate glass compositions than has been reported previously.

## II. Experimental Procedures

Raw materials including stoichiometric $FePO_4 \cdot xH_2O$ (100%, Alfa Aesar), $Fe_2O_3$ (Alfa Aesar, ≥99%), and $NH_4H_2PO_4$ (Alfa Aesar, 98%, Ward Hill, MA) were used to prepare the crystalline compounds and glasses. Iron phosphate crystalline compounds were prepared following the procedures listed in Table I. Additional details on the preparation and properties of ferric phosphate compounds can be found in Zhang *et al.*[35] X-ray diffraction (Scintag XDS 2000, Scintag, Inc., Cupertino, CA) was used to confirm that the desired, stoichiometic phases were formed. Secondary crystalline phases could not be detected by XRD in any of these samples.

Glasses were prepared from iron phosphate crystalline compounds or batch materials. The melt conditions are summarized in Table II. Some melts with O/P ratios ≥ 4.0 were quenched between steel rollers to avoid crystallization.[19] Other melts with O/P ratios near 3.0 were prepared in sealed silica ampoules to minimize $P_2O_5$-volatilization and to control the iron valence during melting. The ampoules were quenched in water after the designated melt time. Finally, several melts with intermediate [Fe]/[P] ratios were prepared by conventional methods, in air in open alumina crucibles and then quenched on steel plates. In general, the sample sizes were 3–5 g for orthophosphate glasses prepared by the roller quenching method, 0.6–2.5 g for glasses melted in sealed silica ampoules, and 20–40 g for the glasses melted in open crucibles. Every glass was pulverized to ~53 μm and characterized by XRD to confirm the vitreous state. Samples of glass powders were coated by carbon and their Fe/P ratios were determined using the energy-dispersive X-ray spectrometry (EDS) system associated with the Hitachi S4700 scanning electron microscope (Hitachi High-Tech, Tokyo, Japan). These

L. Pinckney—contributing editor

Manuscript No. 28759. Received October 11, 2010; approved February 2, 2011.
This work was supported by the National Science Foundation under Grant No. DMR-0305202 and DMR-0502463.
*Member, The American Ceramic Society.
†Author to whom correspondence should be addressed. e-mail: brow@mst.edu

**Table I. Conditions Used to Prepare the Iron Phosphate Crystalline Compounds**

| Compound | Batch materials | Preparation conditions |
|---|---|---|
| α-$FePO_4$ | $FePO_4 \cdot xH_2O$ | 880°C in air for 12 h |
| $Fe_3(PO_4)_2$-A | $FePO_4$, $Fe_2O_3$ | Reduced in forming gas* at 680–690°C for 6 h |
| $Fe_3(PO_4)_2$-B | $Fe_3(PO_4)_2$-A | 1150°C for 12 h in sealed ampoule |
| $Fe_7(PO_4)_6$ | $Fe_2O_3$, $FeP_2O_6$ | 900°C for 12 h in sealed ampoule |
| $Fe_4(P_2O_7)_3$ | $FePO_4$, $Fe(PO_3)_3$ | 800°C in air for 12 h, then 940°C in air for 24–48 h |
| $Fe_2P_2O_7$ | $FePO_4$ | Reduced in forming gas* at 560°C for 6 h |
| $Fe_3(P_2O_7)_2$ | $Fe(PO_3)_3$, $Fe_2PO_5$ | 900°C for 12 h in sealed ampoule |
| $Fe_7(P_2O_7)_4$ | $Fe_2P_2O_7$, $Fe_3(P_2O_7)_2$ | 900°C for 12 h in sealed ampoule |
| $Fe(PO_3)_3$ | $Fe_2O_3$, $NH_4H_2PO_4$ | Ammonia burn-off at 500°C overnight, held in air at 800°C for 12 h |
| $Fe(PO_3)_2$ | $FePO_4$, $NH_4H_2PO_4$ | Ammonia burn-off at 500°C overnight, then reduced in forming gas* at 650°C for 6 h |

*Forming gas is 10% $H_2$ and 90% Ar.

analyses were based on an Fe/P calibration curve determined by analyzing the corresponding crystalline compounds. At least five measurements were done on each sample, and the average Fe/P ratio, with one standard deviation, is reported. The $Fe^{2+}/Fe_{tot}$ contents of the glasses were determined by a titration technique using $KMnO_4$ (~2 mM),[36] with an absolute uncertainty of 2%. The Fe/P and $Fe^{2+}/Fe_{tot}$ ratios were then used to calculate the O/P ratio for every glass. EDS analyses indicated that these glasses possessed <2 mol% $Al_2O_3$ (or $SiO_2$) as a contaminant from the crucible (or ampoule). There was no evidence for these contaminants affecting the Raman spectra of the glasses, and their presence is ignored in discussions of glass compositions and structures.

An Horiba–Jobin Yvon LabRam-HR spectrometer (Horiba-Jobin Yvon, Inc., Edison, NJ) was used to collect Raman spectra with a He–Ne laser (632.8 nm) as the excitation source. In general, spectra were collected through a ×10 microscope objective from the surfaces of crystalline powders (53 μm particle size) and from the surfaces of fragments of glasses prepared by the various methods.

## III. Results

Table III lists the crystallographic parameters reported in the literature for the iron phosphate crystals prepared in this study. The average P–O bond distances for nonbridging ($P–O_{nb}$) and bridging ($P–O_{br}$) oxygens are indicated. Nonbridging oxygens are those that are linked to one P-tetrahedron in the structure, and bridging oxygens are linked to two P-tetrahedra. Also listed are the average P–O–P bond angles for the crystalline pyro- and metaphosphate compounds.

Table IV summarizes the compositions of the glasses prepared in this work. The O/P ratios were calculated from the measured $Fe^{2+}/Fe_{total}$ ratios, obtained by titration, and the Fe/P ratios obtained by EDS. In general, the O/P ratios differ from their nominal values principally because of a change in the average Fe-redox state after melting.

Figure 1 shows the Raman spectra collected from the crystalline iron orthophosphate (O/P = 4) compounds. The major band near ~1009 $cm^{-1}$ in the spectrum from α-$FePO_4$ is assigned to the symmetric $PO_4$-stretching mode associated with the $Q^0$ $PO_4^{3-}$ tetrahedra.[20,21] For $Fe_3(PO_4)_2$-A and -B, the intense bands between 900 and 980 $cm^{-1}$ are also assigned to the symmetric $PO_4$-stretching modes. The less intense bands between 900 and 1100 $cm^{-1}$ in the spectra from $Fe_7(PO_4)_6$, $Fe_3(PO_4)_2$-A, and $Fe_3(PO_4)_2$-B are assigned to the asymmetric $PO_4$ modes associated with the reduced symmetry of these $PO_4^{3-}$ units.[22] The peaks below 600 $cm^{-1}$ are related to different P–O and Fe–O stretching and bending modes.[21,37]

Figure 1 also shows the Raman spectra collected from the glasses that have nominal compositions near the iron orthophosphate stoichiometry (O/P≈4). The Raman spectra from the O1, O2, and O3 glasses are similar to that obtained from α-$FePO_4$. The spectra from these glasses are dominated by an intense peak centered between 1000 and 1010 $cm^{-1}$, due to the $PO_4$-stretching modes associated with the nonbridging oxygens, and some lower intensity peaks are also present in the range between 200 and 500 $cm^{-1}$, similar to what is seen for α-$FePO_4$. The broader full-widths at half-maximum (FWHM = 30–40 $cm^{-1}$) of the peak near 1000 $cm^{-1}$ and their slightly lower frequencies from the glasses, compared with crystalline $FePO_4$ (FWHM = 10 $cm^{-1}$), are consistent with what was reported by Burba *et al.*[20] for amorphous and crystalline α-$FePO_4$, but differ from those spectral features reported for the orthorhombic form of $FePO_4$. The latter spectra resemble that shown in Fig. 1 for $Fe_3(PO_4)_2$-A. The assignments for the low-frequency peaks in the spectra from the O1, O2, and O3 glasses are the same as those described above for the crystalline samples.

**Table II. Conditions Used to Prepare the Iron Phosphate Glasses**

| Glass | Nominal composition (mole fraction) | Melting vessel | Atmosphere | Temp (°C)/ time (h) | Quench methods |
|---|---|---|---|---|---|
| O1 | $60Fe_2O_3$–$40P_2O_5$ | $Al_2O_3$ crucible | In air | 1200/0.5 h | Roller quench[19] |
| O2 | $52Fe_2O_3$–$48P_2O_5$ | $Al_2O_3$ crucible | In air | 1300/0.5 h | Roller quench[19] |
| O3 | $50Fe_2O_3$–$50P_2O_5$ | $Al_2O_3$ crucible | In air | 1300/2 h | Roller quench[19] |
| P1 | $40Fe_2O_3$–$60P_2O_5$ | $Al_2O_3$ crucible | In air | 1100/2 h | Steel plate quench |
| P2 | $67FeO$–$33P_2O_5$ | $SiO_2$ ampoule | Sealed under vacuum | 1200/2 h | Water quench |
| P3 | $10Fe_2O_3$–$50FeO$–$40P_2O_5$ | $SiO_2$ ampoule | Sealed under vacuum | 1200/3 h | Water quench |
| P4 | $35Fe_2O_3$–$65P_2O_5$ | $Al_2O_3$ crucible | In air | 1200/2 h | Steel plate quench |
| P5 | $31Fe_2O_3$–$69P_2O_5$ | $SiO_2$ ampoule | Sealed in air | 1110/12 h | Water quench |
| P6 | $45Fe_2O_3$–$55P_2O_5$ | $Al_2O_3$ crucible | In air | 1200/2 h | Steel plate quench |
| P7 | $45Fe_2O_3$–$55P_2O_5$ | $Al_2O_3$ crucible | In air | 1150/2 h | Steel plate quench |
| P8 | $41Fe_2O_3$–$59P_2O_5$ | $Al_2O_3$ crucible | In air | 1150/2 h | Steel plate quench |
| M1 | $28Fe_2O_3$–$72P_2O_5$ | $SiO_2$ ampoule | Sealed in air | 1180/12 h | Water quench |
| M2 | $25Fe_2O_3$–$75P_2O_5$ | $SiO_2$ ampoule | Sealed in air | 1250/4 h | Water quench |
| M3 | $50FeO$–$50P_2O_5$ | $SiO_2$ ampoule | Sealed under vacuum | 1200/2 h | Water quench |
| M4 | $50FeO$–$50P_2O_5$ | $SiO_2$ ampoule | Sealed under vacuum | 1200/0.5 h | Water quench |

**Table III. Crystallographic Parameters Reported for the Crystalline Iron Phosphates**

| Compound | Space group | Average P–$O_{nb}$ (Å)† | Average P–$O_{br}$ (Å)† | P–O–P bond angle | References |
|---|---|---|---|---|---|
| $FePO_4$ | $P3_121$ | 1.530 | — | — | Goiffon *et al.*[45] |
| $Fe_3(PO_4)_2$-A | $P2_1/c$ | 1.537 | — | — | Warner *et al.*[46] |
| $Fe_3(PO_4)_2$-B | $P2_1/c$ | 1.540 | — | — | Warner *et al.*[47] |
| $Fe_7(PO_4)_6$ | $P\bar{1}$ | 1.543 | — | — | Gorbunov *et al.*[48] |
| $Fe_4(P_2O_7)_3$ | $P2_1/n$ | 1.514 | 1.575 | 155.7° | Elbouaanani *et al.*[49] |
| $Fe_2P_2O_7$ | $C\bar{1}$ | 1.519 | 1.554 | —‡ | Hoggins *et al.*[50] |
| $Fe_3(P_2O_7)_2$ | Pnma | 1.506 | 1.593 | 135.2° | Ijjaali *et al.*[51] |
| $Fe_7(P_2O_7)_4$ | $C222_1$ | 1.512 | 1.596 | 136.5° | Malaman *et al.*[52] |
| $Fe(PO_3)_3$ | Ic | 1.484 | 1.577 | 143°§ | Rojo *et al.*[53] |
| $Fe(PO_3)_2$ | $C2/c$ | 1.485 | 1.59 | 137.5° | Genkina *et al.*[54] |

†Nonbridging oxygen bond length and bridging oxygen bond length. ‡No exact P–O–P angles reported. §Estimated based on average of reported smallest (137°) and largest (149°) P–O–P angles.

Figure 2 shows the Raman spectra collected from iron pyrophosphate crystalline compounds (O/P = 3.5). The most intense peaks in each spectrum, between 1000 and 1100 $cm^{-1}$, correspond to the symmetric $PO_3$ vibrations of inequivalent nonbridging oxygens associated with the $Q^1$ $P_2O_7^{4-}$ anions.[23] The less-intense peaks between 1000 and 1200 $cm^{-1}$ are assigned to the asymmetric $PO_3$ modes associated with $Q^1$-tetrahedra. The centrosymmetric $Fe_2P_2O_7$ crystals do not have as many Raman active $PO_3$-stretching modes due to the symmetry of the compound.[23,38] Compared with $Fe_2P_2O_7$ and $Fe_7(P_2O_7)_4$, the spectra from the crystalline compounds $Fe_3(P_2O_7)_2$ and $Fe_4(P_2O_7)_3$ have many more peaks assigned to asymmetric $PO_3$ modes (Fig. 2), consistent with the lower symmetry of these latter pyrophosphate units (Table III).

The bands between 700 and 800 $cm^{-1}$ in Fig. 2 are assigned to the symmetric P–O–P-stretching mode associated with the bridging oxygen that links two $Q^1$-tetrahedra in a pyrophosphate anion. Crystalline $Fe_2P_2O_7$ has a relatively intense P–O–P peak near ~731 $cm^{-1}$, which agrees with the spectrum reported in Baran *et al.*[23] For the other iron pyrophosphate crystalline compounds, the intensities of the P–O–P peak are relatively weak. The peak near ~935 $cm^{-1}$ in the spectrum of $Fe_7(P_2O_7)_4$ is assigned to the asymmetric vibration of P–O–P bonds, as is the weak peak near ~1000 $cm^{-1}$ in the spectrum of $Fe_4(P_2O_7)_3$.

Figure 3 shows the Raman spectra collected from glasses with O/P ratio ~3.5. These glasses, with different Fe/P ratios (between 0.65 and 0.83), have similar Raman spectra. In general, the broad peaks in the spectra from the glasses occur at similar frequencies as those from the crystalline pyrophosphates (Fig. 2), and similar assignments can be made for the peaks in the spectra from the glasses. The most intense peak in each spectrum, at frequencies from ~1060 to ~1100 $cm^{-1}$, can be assigned to the $PO_3$-stretching modes associated with the nonbridging oxygens on $Q^1$-tetrahedra.[23] The higher frequency shoulders evident in each spectrum could be due to asymmetric $PO_3$ modes associated with the $Q^1$-tetrahedra, but also could be due to symmetric $PO_2$-stretching modes associated with $Q^2$-tetrahedra. This latter assignment seems particularly obvious for the P5 glass, which has a relatively low O/P ratio (3.16, Table IV) and so should have a greater fraction of $Q^2$-tetrahedra. Likewise, the shoulders near ~1000 $cm^{-1}$ could be assigned to other $PO_3$ modes associated with the $Q^1$-tetrahedra, or to $PO_4$ modes associated with $Q^0$ units in the glasses. The bands between 700 and 800 $cm^{-1}$ are related to the symmetric P–O–P-stretching modes associated with linkages to $Q^1$-tetrahedra. It is interesting that the peak for the P–O–P symmetric-stretching mode has a greater relative intensity for the ferrous P2 glass than for the other glasses. In addition, the peak position varies from 720 $cm^{-1}$ for the P5 glass to 765 $cm^{-1}$ for the P2 glass.

Figure 4 shows the Raman spectra of the crystalline ferric and ferrous metaphosphate (O/P = 3) compounds and several metaphosphate glasses. The $Fe(PO_3)_3$ and $Fe(PO_3)_2$ crystalline compounds have bands at similar frequencies; however, their relative intensities are quite different. The intense peak near ~1196 $cm^{-1}$ in the spectrum from the crystalline ferric compound ($Fe(PO_3)_3$) corresponds to the $PO_2$-stretching modes associated with $Q^2$-tetrahedra,[15,16,24] and the intense peaks at 1160 and 1205 $cm^{-1}$ in the spectrum from the crystalline ferrous compound ($Fe(PO_3)_2$) also correspond to these symmetric $PO_2$-stretching modes associated with inequivalent P–$O_{nb}$ bonds.[25] The less intense bands between 1000 and 1250 $cm^{-1}$ are likely related to the asymmetric $PO_2$-stretching modes.[25,26] The peak for the symmetric-stretching mode of P–O–P bonds that link the $Q^2$-tetrahedra in these crystalline compounds is present at 661 $cm^{-1}$ for $Fe(PO_3)_3$ and at 680 $cm^{-1}$ for $Fe(PO_3)_2$; the relative intensity of the latter peak is significantly greater than the former.

For the glasses in Fig. 4, the major bands between 1150 and 1200 $cm^{-1}$ are assigned to the $PO_2$-stretching modes associated with $Q^2$-tetrahedra. The spectra from glasses M1, M2, and M3 each have a broad peak centered near 1060–1070 $cm^{-1}$. These peaks are most likely due to $PO_3$-stretching modes associated with $Q^1$-tetrahedra that terminate phosphate chains. The low-intensity peak centered near 1300 $cm^{-1}$ in each spectrum of the metaphosphate glasses is assigned to asymmetric $PO_2$-stretching modes associated with $Q^2$-tetrahedra. The peak due to the P–O–P-stretching modes is present in each spectrum, ranging between

**Table IV. Glass Compositions: the O/P Atom Ratios were Calculated from the Fe/P Atom Ratios, Determined by EDS, and the Fraction of $Fe^{2+}$, Determined by Titration**

| Glass | O1 | O2 | O3 | P1 | P2 | P3 | P4 | P5 |
|---|---|---|---|---|---|---|---|---|
| Fe/P ratio | 1.80±0.10 | 1.04±0.15 | 0.98±0.12 | 0.68±0.07 | 0.92±0.13 | 0.65±0.11 | 0.67±0.03 | 0.45±0.02 |
| $Fe^{2+}/Fe_{total}$ (%) | 35±1 | 50±1 | 51±3 | 16±1 | 95±4 | 64±8 | 22±1 | 7±3 |
| O/P ratio | 4.89±0.10 | 3.78±0.18 | 3.72±0.16 | 3.47±0.12 | 3.45±0.16 | 3.27±0.15 | 3.43±0.04 | 3.16±0.04 |

| Glass | P6 | P7 | P8 | M1 | M2 | M3 | M4 |
|---|---|---|---|---|---|---|---|
| Fe/P ratio | 0.75±0.08 | 0.83±0.11 | 0.73±0.09 | 0.34±0.03 | 0.37±0.07 | 0.51±0.06 | 0.51±0.07 |
| $Fe^{2+}/Fe_{total}$ (%) | 30±2 | 23±2 | 16±17 | 5±2 | 17±4 | 81±4 | 97±1 |
| O/P ratio | 3.51±0.11 | 3.66±0.16 | 3.53±0.14 | 3.03±0.04 | 3.02±0.10 | 3.06±0.07 | 3.02±0.07 |

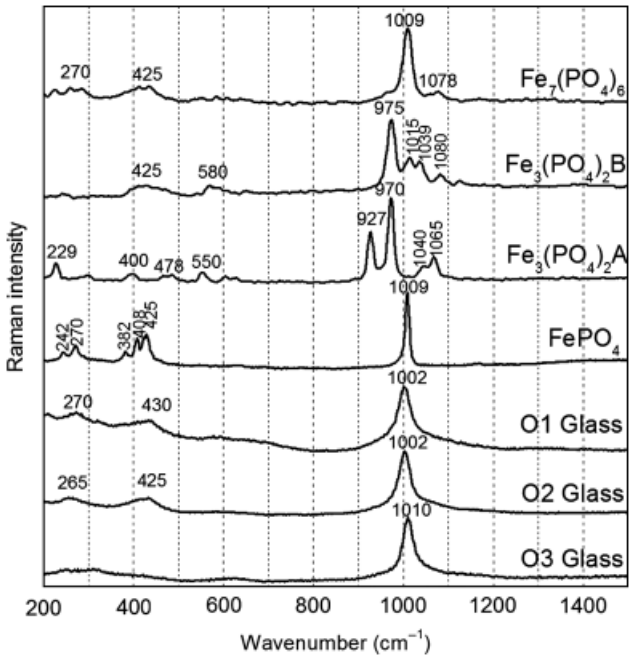


**Fig. 1.** Raman spectra of iron orthophosphate crystals and glasses.

683 cm$^{-1}$ (M4) and 720 cm$^{-1}$ (M1). The relative intensity of this peak varies considerably with composition.

## IV. Discussion

### *(1) Peak Assignments and Phosphate Tetrahedral Distributions*

Table V summarizes the Raman peak assignments for the various samples. The assignments are consistent with previous Raman spectroscopic studies of phosphate crystalline compounds and glasses.[11–34,37,38] The peaks below 600 cm$^{-1}$ are related to network bending modes,[17,21,37] which are not individually assigned in this paper. The peak positions vary systematically with phosphate chemistry, with the frequency (wave numbers) of the P–O-stretching modes increasing in the order orthophosphate < pyrophosphate < metaphosphate. The Raman frequencies for iron

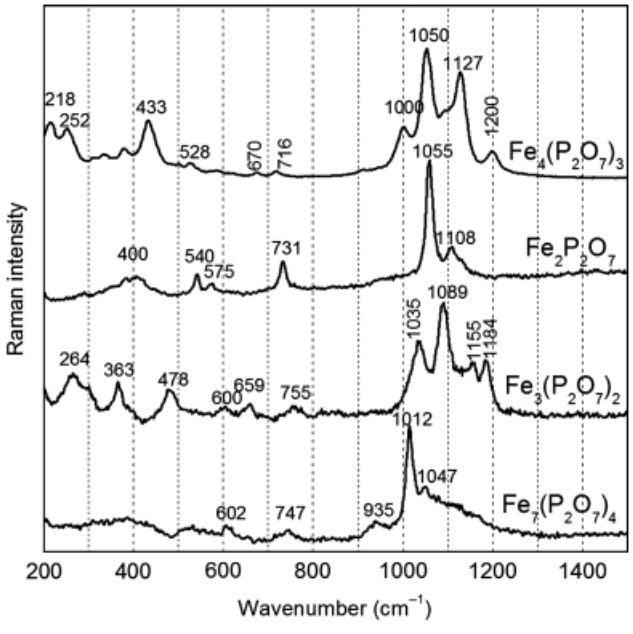


**Fig. 2.** Raman spectra of crystalline iron pyrophosphate compounds.

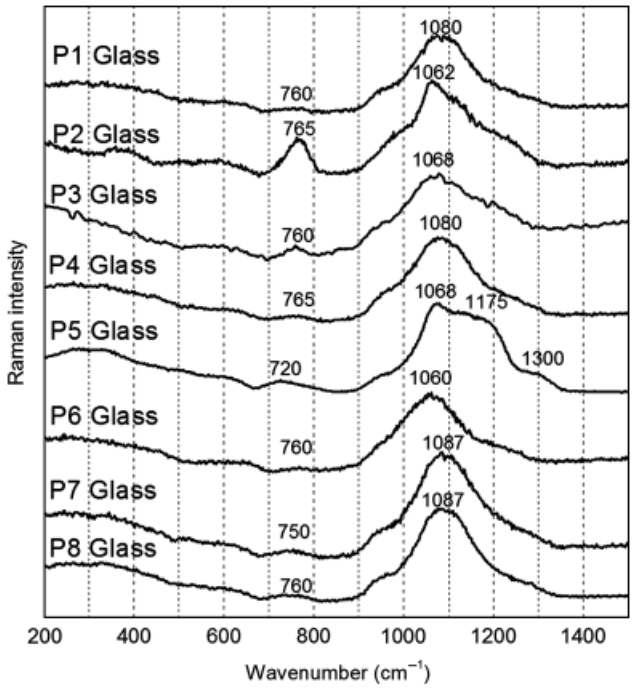


**Fig. 3.** Raman spectra of glasses melted from pyrophosphates compounds.

phosphate glasses fall into similar ranges with the corresponding iron phosphate crystalline compounds, indicating some structural similarity between the glassy and corresponding crystalline phosphate compounds. For example, the similarity in the Raman spectra from the roller-quenched "orthophosphate glasses" to that collected from α-$FePO_4$ indicates that the structure of this quartz-like compound, based on tetrahedral ($PO_4$) and ($FeO_4$) units, is a better model for the glass structure than the orthorhombic form of $FePO_4$ with its structure based on ($PO_4$) and ($FeO_6$) units.[20]

It is obvious that the relative contributions of the various P–O-stretching modes in the range of 900 and 1400 cm$^{-1}$ change with glass composition. To quantify these changes, each spectrum

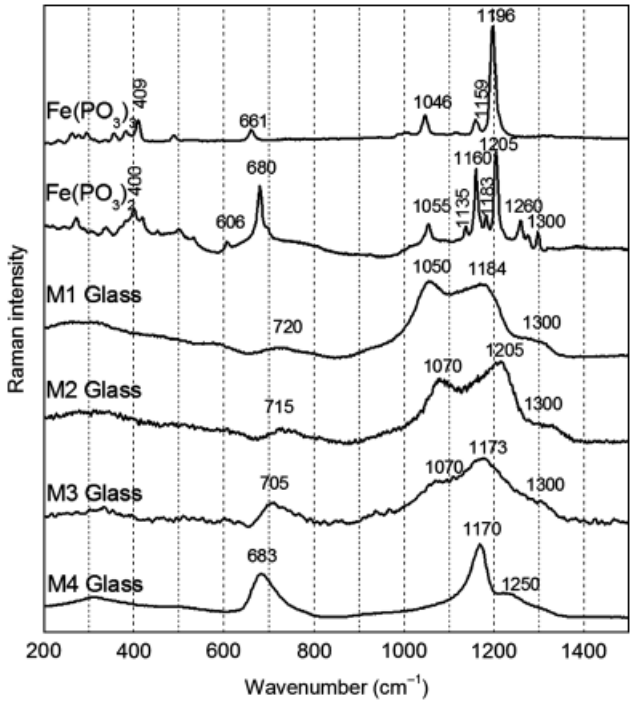


**Fig. 4.** Raman spectra of iron metaphosphate crystals and glasses.

**Table V. Summary of Raman Frequency Ranges ($cm^{-1}$) Related to Various Phosphate Groups in Iron Phosphate Crystalline Compounds and Glasses**

| Compounds | Glasses | Assignment |
|---|---|---|
| 200–600 | 200–600 | Network bending |
| 660–680 | 680–720 | P–O–P symmetric stretch ($Q^2$) |
| 710–760 | 720–780 | P–O–P symmetric stretch ($Q^1$) |
| 960–1010 | 990–1010 | $PO_4$ symmetric stretch ($Q^0$) |
| 1010–1100 | 1030–1100 | $PO_3$ symmetric stretch ($Q^1$) |
| 1120–1200 | ~1200 | $PO_3$ asymmetric stretch ($Q^1$) |
| 1150–1210 | 1050–1220 | $PO_2$ symmetric stretch ($Q^2$) |
| 1260–1300 | 1250–1310 | $PO_2$ asymmetric stretch ($Q^2$) |

was fit by four Gaussian curves centered near ~950–990, ~1040–1090, ~1120–1200, and ~1250–1320 $cm^{-1}$. The peak positions and FWHM of these curves were allowed to vary until a best-fit solution was achieved. An example of one fit, for the P4 glass, is shown in Fig. 5.

The relative intensities of the four peaks are plotted as a function of the O/P ratio for each of the iron phosphate glasses in Fig. 6. The relative intensities of the peaks near 1180 and near 1300 $cm^{-1}$ both decrease with increasing O/P ratio and the relative intensity of the peak centered near 1070 $cm^{-1}$ increases, reaching a maximum at O/P ~ 3.5, before decreasing with greater O/P ratio. The relative intensity of the peak near 970 $cm^{-1}$ remains low for O/P < 3.3, but becomes the dominant peak for glasses with O/P > 3.5.

Assignments of these four peaks to specific structural units in the glass are not unambiguous. It is likely, for example, that the Raman peak near 1180 $cm^1$ for glasses with O/P ratios between 3.0 and 3.5 will have overlapping contributions from symmetric $PO_2$-stretching modes associated with $P–O_{nb}$ bonds on $Q^2$-tetrahedra, and asymmetric $PO_3$-stretching modes associated with $P–O_{nb}$ bonds on $Q^1$-tetrahedra; see, for example, the spectra from crystalline $Fe_4(P_2O_7)_3$ and $Fe_3(P_2O_7)_2$ in Fig. 2, with peaks at 1150–1200 $cm^{-1}$ associated with the $P_2O_7^{4-}$ anions. Nevertheless, the trends in peak intensity in Fig. 6 can be interpreted using well-known phosphate structural chemistry models if the peaks near 1180 and 1300 $cm^{-1}$ are assigned to the symmetric and asymmetric $PO_2$-stretching modes associated with $P–O_{nb}$ bonds on $Q^2$-tetrahedra, respectively, the peak centered near 1070 $cm^{-1}$ is assigned to $PO_3$-stretching modes associated with $P–O_{nb}$ bonds on $Q^1$-tetrahedra, and the peak centered near 970 $cm^{-1}$ is assigned to $PO_4$-stretching modes associated with $P–O_{nb}$ bonds on $Q^0$-tetrahedra. The solid lines in Fig. 6 show the predicted compositional dependences of the distributions of $Q^x$-tetrahedra, assuming the simplest chemical model in which $Q^2$-tetrahedra convert to $Q^1$-tetrahedra, which then convert to $Q^0$-tetrahedra, with increasing O/P ratio.[10] In general, the relative intensities of the peaks centered at 1180, 1070, and 970 $cm^{-1}$ change in the same qualitative way as the predicted fractions of $Q^2$, $Q^1$, and $Q^0$-tetrahedra, respectively. (The compositional

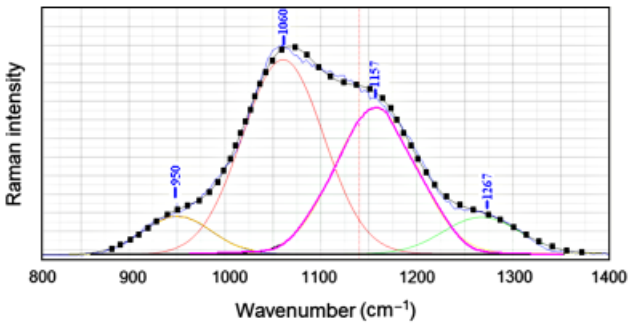


**Fig. 5.** Decomposition of the Raman spectrum (blue line) for the P4 glass into four Gaussian peaks, the sum of which is indicated by the dotted line.

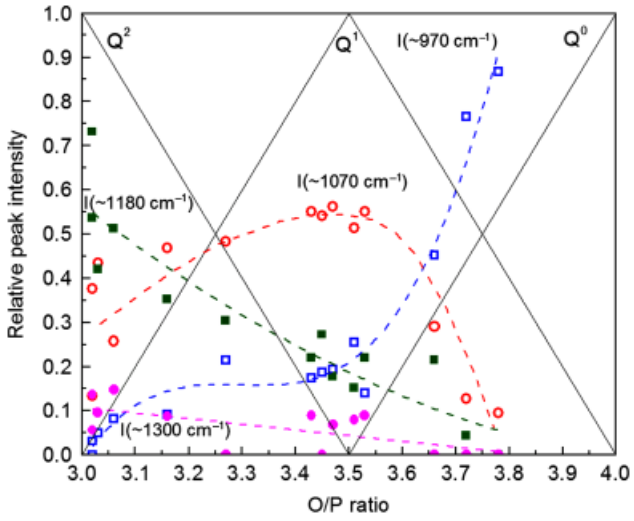


**Fig. 6.** Relative intensities of the four Gaussian peaks used to fit the Raman spectra in the range 900–1400 $cm^{-1}$ from each iron phosphate glass. The peak positions are (□) 950–990 $cm^{-1}$, (○) 1040–1090 $cm^{-1}$, (■) 1120–1200 $cm^{-1}$, (●) 1250–1320 $cm^{-1}$. Solid lines are the predicted $Q^x$ distributions assuming a chemically simple model.[10] Dashed lines are guides for the eye.

dependence of the relative intensity of the peak near 1250–1320 $cm^{-1}$ parallels that of the 1180 $cm^{-1}$ peak, supporting the assignment of the former to asymmetric-vibrational modes on nonbridging oxygens on $Q^2$-tetrahedra.) Similar spectral trends have been reported from Raman studies of other polyphosphate glasses, including Li-phosphates,[27] Zn-phosphates,[13,28] Ca-, and Mg-phosphates.[29]

The Raman spectra of the iron phosphate glasses are more complex than can be explained by the "chemically simple" structural model, shown in Fig. 6. For example, the spectra collected from glasses like P1, P2, and P3 have peaks or shoulders that indicate the concomitant presence of $Q^0$-, $Q^1$-, and $Q^2$-tetrahedra for pyrophosphate compositions that should possess mostly $Q^1$-tetrahedra. Similar features in the Raman spectra from Zn-polyphosphate[13] and Pb-polyphosphate[30] glasses were interpreted using the Van Wazer site distribution model[31] for the phosphate melts that rely on the following disproportionation reaction:

$$2Q^1 \leftrightarrow Q^2 + Q^0 \quad (1)$$

It has been shown that increasing the field strength of metal cations in a polyphosphate melt shifts the site distribution reaction to the right, increasing the structural complexity of the resulting glasses.[32,39] Obtaining quantitative measurements of the site distributions from the Raman spectra is difficult, not least because of overlapping peaks due to the different symmetric- and asymmetric-stretching modes associated with the different tetrahedra. However, the comparison of the relative peak intensities with the predicted $Q^x$-distributions in Fig. 6 is qualitatively consistent with the site disproportionation model for compositions around the pyrophosphate stoichiometry. It seems clear, then, that to understand the effects of composition on the properties of iron phosphate glasses, the role of a broad distribution of different phosphate anions must be considered.

This interpretation of the Raman spectra of iron phosphate glasses with compositions around the pyrophosphate stoichiometry is consistent with what has been proposed by others for similar glasses.[9,17,18] That is, $Q^1$-tetrahedra dominate the phosphate anions that constitute the structures of these glasses, with $Q^0$-and $Q^2$-tetrahedra also present. The relative concentrations of the latter tetrahedra depend on the O/P ratio of the glass and may depend on thermal history if reaction (1) is treated as an equilibrium reaction.[31,32]

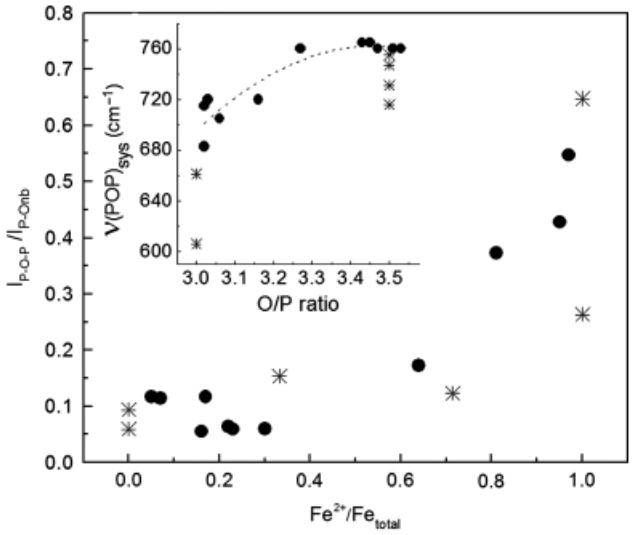


**Fig. 7.** Intensity ratios for the P–O–P (600–800 $cm^{-1}$) and P–$O_{nb}$ (peak between ~1000 and 1200 $cm^{-1}$) symmetric stretching Raman peaks for iron phosphate crystalline compounds (*) and glasses (●) as a function of the fraction of ferrous ions. The inset shows the frequency of the $(POP)_{sym}$ peak as a function of composition. The dashed line is a guide for the eye.

The Raman spectra from more complex iron phosphate glasses, for example, those containing other oxides, can be interpreted in a similar manner, if the effects of the field strengths of other cations are considered. For example, lower-field strength cations generally shift the Raman peak frequencies for P–$O_{nb}$-stretching modes to lower wave numbers,[11,12] and the addition of other oxides may change local symmetries enough to change the relative intensities of symmetric and asymmetric peaks from glasses with the same nominal O/P ratio. The cation effect can be seen in the work of Bingham *et al.*,[18] who discuss the Raman spectra from $K_2O$- and BaO-containing iron phosphate glasses. In that study, peaks centered near 470 and 630 $cm^{-1}$ develop and increase in relative intensity as more modifying oxides are added to an iron pyrophosphate base glass, increasing the O/P ratio. There are no comparable peaks in the "modifier free" compositions in the present study, indicating that the new peaks in the spectra reported by Bingham and colleagues, and seen in other modified iron phosphate glasses[40] with relatively high O/P ratios (>3.5), are due to vibrational modes associated with orthophosphate anions that are charge balanced by the modifying cations. Similar assignments have been made for the Raman spectra of crystalline alkali iron orthophosphates.[41]

The relative intensity of the P–O–P symmetric-stretching peak between about 600 and 800 $cm^{-1}$ appears to depend on the average oxidation state of the iron ions in these iron phosphate glasses and crystalline compounds. For example, compare the intensity of this peak from the P2 glass (95% $Fe^{2+}$) to that from the P1 glass (16% $Fe^{2+}$) in Fig. 3. Both glasses have similar O/P ratios, but the former glass has a much more intense peak at 765 $cm^{-1}$. Similarly, the relative intensity of the P–O–P symmetric-stretching peak at 683 $cm^{-1}$ for the M4 glass (97% $Fe^{2+}$) is much greater than that for the M1 glass (5% $Fe^{2+}$) (Fig. 4). Figure 4 also shows that the relative intensity of the P–O–P symmetric-stretching peak from crystalline ferrous metaphosphate, $Fe(PO_3)_2$, is significantly greater than for crystalline ferric metaphosphate, $Fe(PO_3)_3$.

Figure 7 plots the ratio of the intensity of the Raman peak due to the P–O–P symmetric stretch, relative to the most intense peak due to the P–$O_{nb}$-stretching modes, as a function of the $Fe^{2+}/Fe_{tot}$ ratio; the P–O–P peak intensity increases with an increasing fraction of ferrous ions, particularly when $Fe^{2+}/Fe_{tot}$ exceeds ~0.6. Changes in Raman peak intensities in phosphate glasses have been related to the degree of covalency in the P–O bond associated with the relevant vibration,[13,33] but those studies involved the effects of cation interactions on the P–$O_{nb}$-stretching modes, not the P–O–P-stretching modes, where the influence of neighboring ferrous or ferric ions is expected to be less. It is unclear why the presence of ferrous ions is associated with an increase in the relative intensity of this peak, although it is clearly evident for both pyrophosphate and metaphosphate glasses and crystals. A low intensity $(POP)_{sym}$ peak has been noted in the Raman spectrum of $SrFe_2(P_2O_7)_2$, but no explanation for this was offered.[34]

The frequency of the $(POP)_{sym}$ peak is lower for crystalline iron metaphosphates (e.g., 680 $cm^{-1}$ for $Fe(PO_3)_2$, Fig. 4) than for the crystalline pyrophosphates (e.g., 731 $cm^{-1}$ for $Fe_2P_2O_7$, Fig. 2). The inset to Fig. 7 shows that for the iron phosphate glasses, there is a systematic increase in the frequency of this peak as the O/P ratio increases. These peaks are too broad (and in some cases, the intensities are too low) to distinguish separate peaks due to $Q^1$-and $Q^2$-linkages, as can be seen in the Raman spectra of Zn-[13] and Pb-polyphosphate glasses.[30] Nevertheless, this systematic change in the frequency of the $(POP)_{sym}$ peak can be related to systematic changes in the nature of the P–O–P linkages, as discussed below.

### *(2) P–O Bond Distances*

The systematic changes in the Raman peak positions can provide additional information about the structures of the iron phosphate glasses and crystalline compounds. Rouse *et al.*[11] indicated that the Raman frequency of the $PO_2$ symmetric-stretching mode for a series of metaphosphate glasses depends on the bond force constant between the modifying metal cation and the nonbridging oxygens (greater force constant, higher Raman peak frequency), and on the size of the modifying metal cation, which affects the O–P–O intratetrahedral bond angles (larger cations increase the bond angle and decrease the Raman peak frequency). A similar effect can be seen in Fig. 4, where the $PO_2$ peak positions for the two metaphosphate glasses dominated by greater field strength ferric ions (M1, 1184 $cm^{-1}$ and M2, 1205 $cm^{-1}$) are at greater frequencies than those of the two "ferrous" metaphosphate glasses (M3, 1173 $cm^{-1}$ and M4, 1170 $cm^{-1}$).

Popović *et al.*[16] has related similar peak shifts to changes in P–O bond lengths, with shorter bonds corresponding to greater Raman frequencies. By comparing the Raman spectra from more than 20 inorganic crystalline phosphates, including ortho-, pyro-, and metaphosphates, Popović developed an empirical relationship that correlates the position of the P–O-stretching mode ($\nu$ in $cm^{-1}$) with the P–O bond lengths ($R$ in Å)[16]

$$\nu = 6.3 \times 10^3 - (3.43 \times 10^3)R \quad (2)$$

Equation (2) produces bond length predictions from Raman frequencies with uncertainties of ±0.01 Å for alkali and alkaline earth phosphates, and Popović indicated that similar predictions could be made for amorphous materials.

Equation (2) is plotted in Fig. 8, along with the corresponding *average* P–O bond lengths (Table III) and the average Raman peak positions for the iron phosphate crystalline compounds analyzed in this study. There is good agreement between the measured and predicted dependences of the Raman peak positions on the average P–O bond lengths for the P–O-stretching modes associated with nonbridging oxygens on the $Q^0$-, $Q^1$-, and $Q^2$-tetrahedra. However, the Raman frequencies for the P–O–P-stretching modes generally fall below those predicted from the reported average P–O–P bond lengths of the crystalline pyro- and metaphosphate compounds. This discrepancy may be due to the inability to detect and assign the peaks due to asymmetric P–O–P-stretching modes, which should fall in the range of 900–1000 $cm^{-1}$ and so should increase the average peak position to the range predicted by Popović.

Equation (2) was used to predict the average P–$O_{nb}$ and P–$O_{br}$ bond distances for the iron phosphate glasses, using the most intense peak in the range from 1000 to 1300 $cm^{-1}$ for the

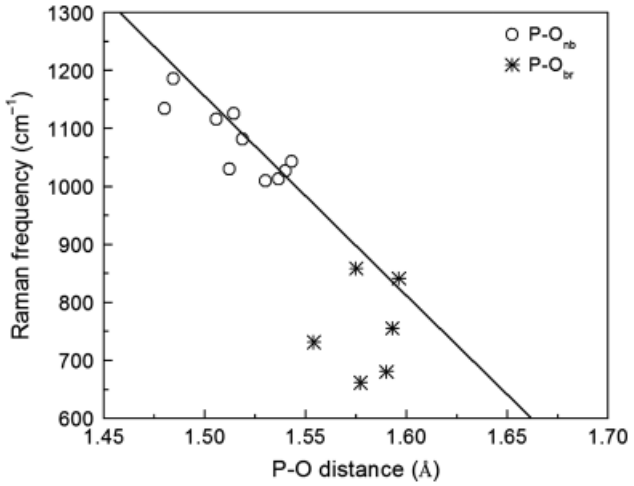


**Fig. 8.** The average positions of the Raman peaks for the P–$O_{nb}$ (○) and P–$O_{br}$ (∗) stretching modes, compared with the average respective bond distances, for the iron phosphate crystalline compounds studied in this work. The line is the empirical correlation (Eq. (2)) proposed by Popović *et al.*[16]

former, and the peak due to the P–O–P-symmetric stretch in the 600–800 $cm^{-1}$ range for the latter. These bond distances are reported as a function of O/P ratio in Fig. 9. In general, it appears that the average P–$O_{nb}$ bonds become longer and the average P–$O_{br}$ bonds become shorter as the O/P ratio increases. Also plotted are the *overall average* P–O bond lengths, calculated from a weighted average of P–$O_{nb}$ and P–$O_{br}$ distances for each respective glass. The overall average P–O bond distance decreases slightly, from 1.57 to 1.54 Å, with increasing O/P ratio, as nonbridging oxygens replace bridging oxygens. The open symbols in Fig. 9 report the average P–O bond distances from X-ray and neutron diffraction studies of ferrous metaphosphate[42] and ferric polyphosphate glasses.[43,44] Overall, there is reasonable agreement between the P–O bond distances predicted from the Raman spectra and those reported from the diffraction studies, although the former are consistently ∼0.02 Å longer than the latter. This difference is likely associated with the assumptions made in the use of the Popović relationship.

## V. Summary

Raman spectra collected from crystalline ferrous, ferric, and ferrous-ferric phosphate compounds and glasses provide information about the phosphate anions that constitute the structures of these materials. In general, the glasses have structures that are similar to crystals with similar stoichiometries, although the glass structures are complicated by the presence of broader distributions of phosphate anions, produced by disproportionation of chain-terminating ($Q^1$) units to form isolated ($Q^0$) and chain-linking ($Q^2$) tetrahedra. Systematic changes in Raman peak positions with glass compositions can be related to changes in the numbers of bridging and nonbridging oxygens, which lead to changes in the average P–O bond distances.

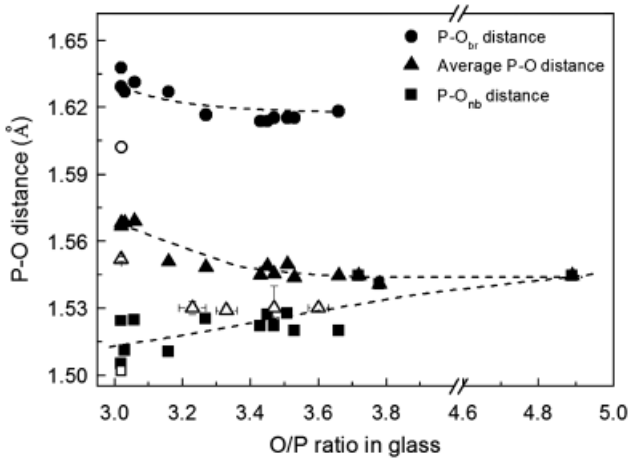


**Fig. 9.** P–O bond distances (closed symbols) for the iron phosphate glasses calculated from Raman peak positions using Eq. (2). The open symbols are bond distances reported in the literature.[42–44] Dashed lines are guides for the eye.

## Acknowledgments

The authors are very grateful to Prof. Mark E. Schlesinger (Missouri S&T) for his assistance with the preparation of the crystalline iron phosphate compounds and Mr. Jong Wook Lim (Missouri S&T) for his help with the collection of the Raman spectra.

## References

[1]J. E. Miller, M. M. Gonzales, L. Evans, A. G. Sault, C. Zhang, R. Rao, G. Whitwell, A. Maiti, and D. King-Smith, "Oxidative Dehydrogenation of Ethane over Iron Phosphate Catalysts," *Appl. Catal. A: Gen.*, **231** [1] 281–92 (2002).
[2]M. M. Gadgil and S. K. Kulshreshtha, "Study of $FePO_4$ Catalyst," *J. Solid State Chem.*, **111**, 357–64 (1994).
[3]A. K. Padhi, K. S. Nanjundaswamy, and J. B. Goodenough, "Phospho-Olivines as Positive-Electrode Materials for Rechargeable Lithium Batteries," *J. Electrochem. Soc.*, **144** [4] 1188–94 (1997).
[4]A. Yamada, S. C. Chung, and K. Hinokuma, "Optimized $LiFePO_4$ for Lithium Battery Cathodes," *J. Electrochem. Soc.*, **148**, A224–9 (2001).
[5]Y.-S. Hong, Y. J. Park, K. S. Ryu, and S. H. Chang, "Crystalline $Fe_3PO_7$ as an Electrode Material for Lithium Secondary Batteries," *Solid State Ion.*, **156** [1-2] 27–33 (2003).
[6]M. G. Mesko and D. E. Day, "Immobilization of Spent Nuclear Fuel in Iron Phosphate Glass," *J. Nucl. Mater.*, **273**, 27–36 (1999).
[7]X. Yu, D. E. Day, G. J. Long, and R. K. Brow, "Properties and Structure of Sodium–Iron Phosphate Glasses," *J. Non-Cryst. Solids*, **215**, 21–31 (1997).
[8]G. K. Marasinghe, M. Karabulut, C. S. Ray, D. E. Day, M. G. Shumsky, W. B. Yelon, C. E. Booth, P. G. Allen, and D. K. Shuh, "Structural Features of Iron Phosphate Glasses," *J. Non-Cryst. Solids.*, **222**, 144–52 (1997).
[9]X. Fang, C. S. Ray, A. Moguš-Milanković, and D. E. Day, "Iron Redox Equilibrium, Structure and Properties of Iron Phosphate Glasses," *J. Non-Cryst. Solids*, **283**, 162–72 (2001).
[10]R. K. Brow, "Review: The Structure of Simple Phosphate Glasses," *J. Non-Cryst. Solids*, **263/264**, 1–28 (2000).
[11]G. B. Rouse, P. J. Miller, and W. M. Risen, "Mixed Alkali Glass Spectra and Structure," *J. Non-Cryst. Solids*, **28**, 193–207 (1978).
[12]B. N. Nelson and G. J. Exarhos, "Vibrational Spectroscopy of Cation-Site Interactions in Phosphate Glasses," *J. Chem. Phys.*, **71** [7] 2739–47 (1979).
[13]R. K. Brow, D. R. Tallant, S. T. Myers, and C. C. Phifer, "The Short Range Structure of Zinc Phosphate Glass," *J. Non-Cryst. Solids*, **191**, 45–55 (1995).
[14]J. J. Hudgens, R. K. Brow, D. R. Tallant, and S. W. Martin, "Raman Spectroscopy Study of the Structure of Lithium and Sodium Ultraphosphate Glasses," *J. Non. Cryst. Solids*, **223** [1,2] 21–31 (1998).
[15]A. Rulmont, R. Cahay, M. Liegeois-Duyckaerts, and P. Tarte, "Vibrational Spectroscopy of Phosphates: Some General Correlations between Structure and Spectra," *Eur. J. Solid State Inorg. Chem.*, **28**, 207–19 (1991).
[16]L. Popović, D. de Waal, and J. C. A. Boeyens, "Correlation between Raman Wavenumbers and P–O Bond Lengths in Crystalline Inorganic Phosphates," *J. Raman Spectrosc.*, **36**, 2–11 (2005).
[17]A. Mogus-Milankovic, B. Pivac, K. Furic, and D. E. Day, "Structural Study of Iron Phosphate Glasses," *Phys. Chem. Glasses*, **38** [2] 74–8 (1997).
[18]P. A. Bingham, R. J. Hand, O. M. Hannant, S. D. Forder, and S. H. Kilcoyne, "Effects of Modifier Additions on the Thermal Properties, Chemical Durability, Oxidation State and Structure of Iron Phosphate Glasses," *J. Non-Cryst. Solids*, **355** [28–30] 1526–38 (2009).
[19]L. Zhang, R. K. Brow, M. E. Schlesinger, L. Ghussn, and E. D. Zanotto, "Glass Formation from Iron-Rich Phosphate Melts," *J. Non-Cryst. Solids*, **356**, 252–7 (2010).
[20]C. M. Burba, J. M. Palmer, and B. S. Holinsworth, "Laser-induced Phase Changes in Olivine $FePO_4$: A Warning on Characterizing $LiFePO_4$-Based Cathodes with Raman Spectroscopy," *J. Raman Spectrosc.*, **40**, 225–8 (2009).
[21]M. P. Pasternak, G. Kh.Rozenberg, A. P. Milner, M. Amanowicz, T. Zhou, U. Schwarz, K. Syassen, R. Dean Miller, M. Hanfland, and K. Brister, "Pressure-induced Concurrent Transformation to an Amorphous and Crystalline Phase in Berlinite-Type $FePO_4$," *Phys. Rev. Lett.*, **79** [22] 4409–12 (1997).
[22]W. H. Baur, "The Geometry of Polyhedral Distortions. Predictive Relationships for the Phosphate Group," *Acta Cryst. B*, **30**, 1195–215 (1974).
[23]E. J. Baran, I. L. Botto, and A. G. Nord, "The Vibrational Spectrum and the Conformation of the $P_2O_7^{4-}$ Anion in $Fe_2P_2O_7$," *J. Mol. Struct.*, **143**, 151–4 (1986).
[24]S. H. Morgan, R. H. Magruder, and E. Silberman, "Raman Spectra of Rare-Earth Phosphate Glasses," *J. Am. Ceram. Soc.*, **70**, C378–80 (1987).
[25]K. Viswanathan, V. U. Nayar, and G. Aruldhas, "Infrared and Raman Spectra of Three Tetrametaphosphates $M_2P_4O_{12}$ ($M$ = Fe, Ni, Zn)," *J. Chem. Sci.*, **95** [5–6] 463–9 (1985).
[26]W. Zhou, W. He, X. Zhang, J. Liu, Y. Du, S. Yan, X. Tian, X. Sun, X. Han, and Y. Yue, "Simple and Rapid Synthesis of $Fe(PO_3)_3$ by Microwave Sintering," *J. Chem. Eng. Data*, **54**, 2073–6 (2009).

[27]M. Tatsumisago, Y. Kowada, and T. Minami, "Raman Spectra of Rapidly Quenched Glasses and Melts Containing Large Amounts of $Li_2O$," *J. Non-Cryst. Solids*, **150**, 207–11 (1992).

[28]H. Takebe, Y. Baba, and M. Kuwabara, "Dissolution Behavior of $ZnO$–$P_2O_5$ Glasses in Water," *J. Non-Cryst. Solids*, **352**, 3088–94 (2006).

[29]M. A. Karakassides, A. Saranti, and I. Koutselas, "Preparation and Structural Study of Binary Phosphate Glasses with High Calcium and/or Magnesium Content," *J. Non-Cryst. Solids*, **347** [1–3] 69–79 (2004).

[30]G. LeSaout, P. Simon, F. Fayon, A. Blin, and Y. Vaills, "Raman and Infrared Study of $(PbO)_x(P_2O_5)_{(1-x)}$ Glasses," *J. Raman Spectrosc.*, **33**, 740–6 (2002).

[31]J. R. Van Wazer, *Phosphorus and its Compounds*. Interscience, New York, NY, 1958.

[32]T. R. Meadowcraft and F. D. Richardson, "Structural and Thermodynamic Aspects of Phosphate Glasses," *Trans. Faraday Soc.*, **61**, 54–70 (1965).

[33]J. Koo, B.-S. Bae, and H.-K. Na, "Raman Spectroscopy of Copper Phosphate Glasses," *J. Non-Cryst. Solids*, **212**, 173–9 (1997).

[34]E. J. Baran, R. C. Mercader, A. Massaferro, and E. Kremer, "Vibrational and $^{57}$Fe-Mössbauer Spectra of Some Mixed Cation Diphosphates of the Type $M^{II}Fe_2^{III}(P_2O_7)_2$," *Acta Part A*, **60**, 1001–5 (2004).

[35]L. Zhang, M. E. Schlesinger, and R. K. Brow, "Phase Equilibria in the $Fe_2O_3$–$P_2O_5$ System," *J. Am. Ceram. Soc.*, doi: 10.1111/j.1551-2916.2010.04287.x (2011).

[36]S. I. Grishin, J. M. Bigham, and O. H. Tuovinen, "Characterization of Jarosite Formed upon Bacterial Oxidation of Ferrous Sulfate in a Packed Bed Reactor," *Appl. Environ. Microbiol.*, **54**, 3101–6 (1988).

[37]R. L. Frost, T. Kloprogge, M. L. Weier, W. N. Wayde, Z. Ding, and G. H. Edwards, "Raman Spectroscopy of Selected Arsenates—Implications for Soil Remediation," *Spectrochim. Acta, Part A*, **59**, 2241–6 (2003).

[38]K. Nakamoto, *Infrared and Raman Spectra of Inorganic and Coordination Compounds*. John Wiley & Sons Inc., New York, NY, (1997).

[39]B. C. Sales and L. A. Boatner, "Physical and Chemical Characteristics of Lead-Iron Phosphate Nuclear Waste Glasses," *J. Non-Cryst. Solids*, **79**, 83–116 (1986).

[40]A. Moguš-Milanković, A. Šantić, S. T. Reis, K. Furić, and D. E. Day, "Studies of Lead–iron Phosphate Glasses by Raman, Mössbauer and Impedance Spectroscopy," *J. Non-Cryst. Solids*, **351**, 3246–58 (2005).

[41]G. Butt, N. Sammes, G. Tompsett, A. Smirnova, and O. Yamamoto, "Raman Spectroscopy of Superionic Ti-Doped $Li_3Fe_2(PO_4)_3$ and $LiNiPO_4$ Structures," *J. Power Sources*, **134**, 72–9 (2004).

[42]U. Hoppe, M. Karabulut, E. Metwalli, R. K. Brow, and P. Jóvári, "The Fe–O Coordination in Iron Phosphate Glasses by X-Ray Diffraction with High Energy Photons," *J. Phys.: Condens. Matter*, **15**, 6143–53 (2003).

[43]M. Karabulut, G. K. Marasinghe, C. S. Ray, G. D. Waddill, and D. E. Day, "A High Energy X-ray and Neutron Scattering Study of Iron Phosphate Glasses Containing Uranium," *J. Appl. Phys.*, **87**, 2185–93 (2000).

[44]A. C. Wright, R. N. Sinclair, J. L. Shaw, R. Haworth, G. K. Marasinghe, and D. E. Day, "A Neutron Diffraction Study of the Structure of Iron Phosphate Glasses," *Phys. Chem. Glasses Eur. J. Glass Sci. Technol. B*, **49** [1] 1–7 (2008).

[45]A. Goiffon, J. C. Dumas, and E. Philippot, "Alpha-Quartz Type Phases: Structure of $FePO_4$ and [57]Fe Mossbauer Spectroscopy," *Rev. Chim. Miner.*, **23**, 99–110 (1986).

[46]J. K. Warner, A. K. Cheetham, A. G. Nord, R. B. Von Dreele, and M. Yethiraj, "Magnetic Structure of Iron(II) Phosphate, Sarcopside, $Fe_3(PO_4)_2$," *J. Mater. Chem.*, **2**, 191–6 (1992).

[47]J. K. Warner, A. K. Cheetham, and D. E. Cox, "Determination of Cation Distribution in $NiFe_2(PO_4)_2$ Using Resonant X-ray and Neutron Powder Diffraction," *J. Appl. Cryst.*, **28**, 494–502 (1995).

[48]Y. A. Gorbunov, B. A. Maksimov, Y. K. Kabalov, A. N. Ivashchenko, O. K. Mel'nikov, and N. V. BeloV, "Crystal Structure of $Fe_3^{2+}Fe_4^{3+}[PO_4]_6$," *Dokl. Akad. Nauk SSR*, **254**, 873–7 (1980).

[49]L. K. Elbouaanani, B. Malaman, R. Gérardin, and M. Ijjaali, "Crystal Structure Refinement and Magnetic Properties of $Fe_4(P_2O_7)_3$ Studied by Neutron Diffraction and Mössbauer Techniques," *J. Solid State Chem.*, **163**, 412–20 (2002).

[50]J. T. Hoggins, J. S. Swinnea, and H. Steinfink, "Crystal Structure of $Fe_2P_2O_7$," *J. Solid State Chem.*, **47**, 278–83 (1983).

[51]M. Ijjaali, G. Venturini, R. Gerardin, B. Malaman, and C. Gleitzer, "Synthesis Structure and Physical Properties of a Mixed-Valence Iron Diphosphate $Fe_3(P_2O_7)_2$: First Example of Trigonal Prismatic $Fe^{2+}$ with $O^2$-Ligands," *Eur. J. Solid State Inorg. Chem.*, **28**, 983–98 (1991).

[52]B. Malaman, M. Ijjali, R. Gerardin, G. Venturini, and C. Gleitzer, "$Fe_7(P_2O_7)_4$, a Mixed Valence Iron Diphosphate the Missing Link Between $Fe_2P_2O_7$ and $Fe_3(P_2O_7)_2$," *Eur. J. Solid State Inorg. Chem.*, **29**, 1269–84 (1992).

[53]J. M. Rojo, J. L. Mesa, L. Lezama, and T. Rojo, "Magnetic Properties of the $Fe(PO_3)_3$ Metaphosphate," *J. Solid State Chem.*, **145**, 629–33 (1999).

[54]E. A. Genkina, B. A. Maksimov, and O. K. Melnikov, "Crystal Structure of Iron Tetrametaphosphate $Fe_2P_4O_{12}$ and its Comparison with the Structure of Other $M_2^{2+}$ $PO_4$($M^{2+}$ = Ni, Mg, Cu, Co)," *Sov. Phys. Crystallogr.*, **30**, 885–9 (1985). □